Ultramicroscopy 160 (2016) 168–181

Contents lists available at ScienceDirect

Ultramicroscopy

journal homepage: www.elsevier.com/locate/ultramic

Full length article

# Synchronizing atomic force microscopy force mode and fluorescence microscopy in real time for immune cell stimulation and activation studies

Séverine Cazaux [a,b,c], Anaïs Sadoun [a,b,c], Martine Biarnes-Pelicot [a,b,c], Manuel Martinez [a,b,c], Sameh Obeid [a,b,c,1], Pierre Bongrand [a,b,c,d], Laurent Limozin [a,b,c], Pierre-Henri Puech [a,b,c,*]

[a] Aix Marseille Université, LAI UM 61, Marseille F-13288, France
[b] Inserm, UMR_S 1067, Marseille F-13288, France
[c] CNRS, UMR 7333, Marseille F-13288, France
[d] APHM, Hôpital de la Conception, Laboratoire d'Immunologie, Marseille F-13385, France

ARTICLE INFO

*Article history:*
Received 3 March 2015
Received in revised form
17 September 2015
Accepted 12 October 2015
Available online 19 October 2015

*Keywords:*
Atomic force microscopy
Fluorescence microscopy
Immune cells
Signalling
Activation
Cell mechanics

ABSTRACT

A method is presented for combining atomic force microscopy (AFM) force mode and fluorescence microscopy in order to (a) mechanically stimulate immune cells while recording the subsequent activation under the form of calcium pulses, and (b) observe the mechanical response of a cell upon photoactivation of a small G protein, namely Rac. Using commercial set-ups and a robust signal coupling the fluorescence excitation light and the cantilever bending, the applied force and activation signals were very easily synchronized. This approach allows to control the entire mechanical history of a single cell up to its activation and response down to a few hundreds of milliseconds, and can be extended with very minimal adaptations to other cellular systems where mechanotransduction is studied, using either purely mechanical stimuli or via a surface bound specific ligand.



## 1. Introduction

Atomic force microscopy (AFM) is a surface probe technique that uses a soft cantilever to image surfaces or to measure or apply forces while interacting with them [1]. Over the last 20 years, AFM in force mode has been largely developed for quantitating molecular interactions, from single molecule unbinding or unfolding events [2–4] to single cell detachment from a substrate or from another cell [5–7].

Recently, force measurements have attracted the attention of many immunologists, in particular in the field of adaptive immunity. A key step of the immune response is the detection by T lymphocytes, thanks to their T cell receptor (TCR), of foreign peptides bound to major histocompatibility complex molecules (pMHC) and displayed on the surface of antigen presenting cells (APCs) [8]. AFM has been applied to the determination of the forces that single TCR/pMHC [9] or BCR/antigen [10] can stand, since force has been recently suspected to be a possible regulator of the antigen discrimination by those molecules [11–16]. Alternative techniques, such as Biomembrane Force Probe [17] and flow chamber [18], were also used to dissect the contribution of forces to single molecule recognition of the TCR/pMHC complex, helping to understand the exquisite sensibility and reliability of this molecular system [19,20]. Further, AFM helped to determine the forces that the immune synapse between a T cell and an APC can create or sustend [21,22]. In the recent years, such techniques have become a very important set of tools to dissect the relationship between cellular mechanics, forces and function, in particular in immune cells [23]. Moreover, immune cells are increasingly recognized to have mechanosensory behaviours [24], which may contribute to their remarkable capabilities of foreign peptide detection [25,26]

A delicate issue in examining the relationship between the receptor binding events (i.e. the TCR/peptide/MHC encounter in the context of T cell recognition [8]) and the early biochemical consequences is to detect the precise moment when the molecules contact with sufficient temporal resolution, let alone controlling when that contact takes place (i.e. the initial encounter). In most biological assays, this question is not addressed otherwise than taking as zero time the initial combination of the relevant

* Corresponding author at: Aix Marseille Université, LAI UM 61 / Inserm, UMR_S 1067 / CNRS UMR 7333, Marseille F-13288, France.
*E-mail address:* pierre-henri.puech@inserm.fr (P.-H. Puech).
[1] Present address: Institut FEMTO-ST, UMR6174-CNRS, UFC – 32, Av. de l'Observatoire, F-25044 Besancon, Cedex, France.

http://dx.doi.org/10.1016/j.ultramic.2015.10.014

components, while even in video microscopy experiments cell contact is determined by visual examination of the images or in the case of lymphocyte stimulation, by the detection of a Ca2+ increase [27,28] or Zap70 phosphorylation [29], among other possibilities.

In the field of mechanotransduction, it has become more and more evident that the consequences of a stimulation event have to be followed simultaneously to the stimulation [30], in order to decipher not only the magnitude of the response, but also to describe the entire history of the stimulation [19,31], where potential delays and time modulations of the response in regard to the stimulation could be affected specifically by mutations or drugs, bringing detailed information about the mechanisms at play. One way of following the signalling activity, in real time, is to visualize it using fluorescent reporters (see above).

In this context, AFM has been very rarely reported, to our knowledge, to be used simultaneously to optical fluorescence imaging in cell biology. These techniques are usually combined by successive applications and led to the implementation of new modalities in commercial AFM (such as JPK Overlay, JPK Instruments, or MIRO, Bruker) to allow easy image superpositions. Potential causes of such a non simultaneous use in imaging/force mode are of two main origins: (a) a common knowledge in the AFM community is that gold coated levers are “reacting” to fluorescence excitation light, whether HBO lamps or lasers are used, and (b) that shutters or advanced optical systems such as confocal scanning heads are producing vibrations that may perturb the AFM measurements. A handful of reports present experiments where AFM indentation is performed while recording a fluorescent signal, e.g. calcium fluxes, but no detail is provided about the exact coupling of the two techniques and their synchronization [30,32,33].

In the literature, reports can be found where force measurements are made concomitantly with fluorescence imaging, but they have been mainly performed using micropipette derived systems such as dual micropipette manipulation [34] (where forces are estimated) or Biomembrane Force Probe [19,31] (with a limitation of the maximal forces that can be applied). The problem of external vibrations is essentially the same as for AFM experiments. In micropipettes, the observation of the cellular system is made from the side and far from any optically flat surface. As a consequence, it suffers from two experimental limitations as compared to AFM: (a) it limits the use of high resolution microscopies and high magnification/NA lenses; (b) the positioning of the probe onto the cell's surface is made with a poor lateral accuracy. As a consequence, only whole cell fluorescence signals can be currently studied. In some seminal experiments, the time resolution of the measurements is also relatively low [31] but this was sufficient to reveal very interesting features of the response of cells to mechanical signals such as delays and recovery times. Due to their lower force range, the application of optical tweezers was not considered here and, as such, is not presented.

A major strength of AFM stems from the possibility of using several modalities on the same set-up: imaging, force indentation to investigate cell mechanics and adhesion force measurements over a great range of force values, from single molecules to cell/cell separation [1]. Aside, it can be coupled to advanced surface microscopies such as reflection interference contrast microscopy (RICM, [35]) or total internal reflection fluorescence microscopy (TIRFM, [36]), or to other high resolution microscopies such as confocal [37], allowing to use the power of fluorescence imaging, with a broad range of dyes or reporter molecules, in order to follow a structure (membrane, nucleus, receptor), its dynamics or a cytosolic signal (calcium fluxes, pH variations) in conjunction to the stimulating signal. While the determination of the moment of contact of the lever tip with the tested cell is relatively simple (by detecting a variation of the force felt by the lever), coordinating the signals from fluorescence and AFM can be complicated and complex synchronization could be necessary. To our knowledge, this point was never clearly reported in literature.

We have developed an original technique allowing us to use AFM to mechanically and specifically stimulate, in a controlled manner over time and space, single white blood cells (T cells, macrophages), while following their activation response simultaneously via conventional calcium probes. We describe a coupling signal existing between fluorescence microscopy and AFM, and use it as a timer to synchronize the stimulus and the response of the cell. In a symmetrical approach, we have used a reverse method that allows to submit T cells to controlled photo-stimulations, gaining insight in their mechanical properties, when activating a small GTPase, Rac, in realtime. This method being simple to put in place, and even if limited in terms of temporal resolution, is a first step toward an easy integration between force mode AFM and signaling studies using fluorescent reporters. This opens a way to new strategies to investigate different components of immune cell mechanotransduction.

## 2. Materials and methods

### 2.1. Cells and cell culture

Two cell types were used: (a) human Jurkat T cells (clone E6-1, ATCC TIB-152), as a model for lymphocytes, and (b) murine J774 macrophages (clone J774A.1 ECACC, Salisbury UK, gift from A. Dumêtre, UMD3, AMU, Marseille) as a model for phagocytes. Cells were counted and passaged three times a week, with a 2 min trypsination step for the macrophages, and their viability assessed by the use of Trypan Blue labelling. The cell culture medium (RPMI 1640) and complements (7% FBS, 1% Hepes 1 M, Glutamax, Pen/Strep) were obtained from Gibco (Life technologies). Cells were monthly tested for the presence of mycoplasma.

### 2.2. Reagents

Chemicals were purchased from Sigma-Aldrich: $CaCl_2$ as a salt (#C1016), bovine serum albumin (BSA) as a powder (#A3294), poly-L-lysine (PLL) as a 0.1% water solution (#P8920). PBS (as 10 × sterile solution, w/o $Ca^{2+}/Mg^{2+}$) was purchased from Gibco (Life technologies). Hellmanex was purchased from Hellma Analytics.

### 2.3. Cells loading with calcium reporter

For calcium imaging, the cells were loaded in suspension with the green fluorescent probe Fluo4 (supplied as Fluo4-AM, #F-14201, Molecular Probes) using protocols adapted from provider's ones prior to immobilization on PLL-coated glass coverslides. Such markers are known to report efficiently the intracellular rise of calcium upon stimulation of immune cells by exhibiting an increase in their fluorescence levels. In short, Fluo4-AM (50 μg in 23 μL) and Pluronic F127 (20% final concentration), purchased from Invitrogen, were dissolved in DMSO and mixed in a 1:1 ratio. $5 \times 10^5$ cells were centrifugated in PBS (1000 rpm, 4 min, RT) and resuspended in a final volume of 500 μL, in which 1 μL of the mixture Fluo4-AM/pluronic is introduced to ensure that DMSO concentration during incubation is $< 0.1\%$. After 30 min incubation at 37 °C, protected from light, the cells are gently centrifugated and resuspended in 150 μL of PBS before being plated on the PLL coverslide at RT, where a supplementary resting step of 30 min is respected.

### 2.4. Rac–PA plasmid and cell transfection

The plasmid of photoactivable Rac fused with the fluorophore mVenus (called hereafter Rac–PA) pTriEx-mVenus-PA-Rac1 was a gift from Klaus Hahn (Addgene plasmid #22007) [38]. Jurkat cells were electroporated using Amaxa system (Lonza, program X-001) using 16 μg of plasmid for $10^6$ cells. Cells transfected with Rac–PA plasmid were either kept in RPMI 10% FBS or starved overnight in RPMI 0.2% FBS before the experiment. Non transfected and sham-transfected (no plasmid) cells displayed the same mechanical behaviour as plasmid transfected ones (not shown); the former were used as control in our experiments.

### 2.5. Cells immobilisation

#### 2.5.1. Lymphocytes

Round coverslides (170 μm thick) were (a) washed in 1% Hellmanex solution for 30 min at 60 °C in an ultrasonic bath (b) successively rinsed with pure ethanol and ultra pure water three times (c) washed in ultra pure water for 30 min at 60 °C in an ultrasonic bath (d) successively rinsed with ethanol and ultra pure water three times (e) dried under an argon flux before storage in dust-free environment. Prior to use, a coverslide was activated for 1 min in a residual air plasma cleaner used at maximal power (Harrick Plasma). A puncher-cut reticulated PDMS well (diameter 8 mm; typical height 1 mm) was used to delimit a zone on the activated coverslide; the well was filled with 100 μL of 0.01% poly-L-lysine in ultra pure water and incubated for 30–45 min at RT. Substrates were gently rinsed three times with PBS before seeding diluted Jurkat cells suspensions (labelled with Fluo4 or not) and letting them to adhere during 15–30 min at room temperature. The glass coverslides were gently washed with PBS 1% BSA 1 mM $CaCl_2$ to remove unbound cells. After labelling the PLL zone with a felt pen, the PDMS well was then removed and the slide mounted in a BioCell (JPK Instruments) or Coverslip Holder (JPK Instruments) filled with the same medium. Note that the use of PLL to immobilize cells has been seen to provoke minimal activation levels of the cell lines under study (see below).

#### 2.5.2. Macrophages

J774 cells were detached from culture flasks using a 2 min Trypsin/EDTA treatment at RT, washed by centrifugation and re suspended in culture medium before being seeded onto ethanol/flame-sterilized glass round coverslides in 6 wells plates. They were made to adhere overnight, in culture medium, at 37 °C. Before the experiments, glass coverslides were rinsed to remove unbound cells. The pre-adhered cells were eventually loaded with Fluo4 using the same procedure as for the Jurkat cells, and mounted into the Biocell temperature control system. The final steps are the same as described above for the lymphocytes.

### 2.6. Atomic force microscope/fluorescence set-up

#### 2.6.1. AFM

Measurements were conducted with an AFM (Nanowizard I, JPK Instruments, Berlin) mounted on an inverted microscope (Zeiss Axiovert 200). The AFM head is equipped with a 15 μm *z*-range linearised piezoelectric ceramic scanner and an infra-red laser. The set-up was used in closed loop, constant height feedback mode [9].

Veeco MLCT cantilevers variants (rectangle (B), large triangle (C), small triangle (D) – see Supplementary Fig. 1) were used in this study, either with tip and gold coating on the back side (MLCT-AU), with tip and no gold (MLCT-UC) or without tip and with gold (MLCT-0). Since they were not commercially available, levers without tip and without gold coating were produced by chemical attack of commercial MLCT-0 levers as described in Supplementary information. When needed, for levers with non square-base pyramidal tip, the assumption of a regular pyramidal tip of half angle 15° to the face was used, calculated from provider data. The sensitivity of the optical lever system was calibrated on the glass substrate and the cantilever spring constant by using the thermal noise method [39]. Spring constant were determined *in situ* using built-in routines of the JPK SPM software (JPK Instruments, v3) at the beginning of each experiment, and the same correction factors were used for all levers types as a first approximation [40]. The calibration procedure for each cantilever was repeated up to three times to rule out possible errors, and repeated at the end of some series of experiments. Spring constants were found to be consistently close to the manufacturer's nominal values and the calibration was stable over the experiment duration.

#### 2.6.2. Fluorescence microscopy

The inverted microscope was equipped with 10 ×, 20 × NA0.8 and 40 × NA0.75 lenses (with a supplementary 1.6 lens), and via a C-mount with a firewire CoolSnap HQ2 camera (Photometrics). Bright field images were used to select cells and monitor their morphology during force measurements. The microscope was also equipped with a LED illumination system (Colibri 2, Zeiss). A PC, separate from the AFM, controlled the camera and Colibri using Zen 2011 software (Zeiss) with suitable plugins under MS Windows 7 64 bits. Alternatively, Micromanager software [41] was used to capture simple transmission images on the same computer when fluorescence imaging was not needed.

Diodes coupled with filters were mounted in the LED illumination system for four simultaneous configurations: UV=(diode 365 nm+filter 387/11); B (for blue)=(diode 470 nm+filter 485/20); G (for green)=(diode NWhite 540–580 nm+filter 560/25); R (for red)=(diode 625 nm+filter 650/13); beams combiners=395, 490, 600 nm (respectively). A corresponding quadriband filter set was inserted in the microscope (dichroic and emission filters from F66-888 set, AHF). Alternatively, an HBO lamp (100 W, X-Cite 120) was connected to the LED illumination system via an optical fibre and was used, together with suitable filters sets for FITC and TRITC excitation (Semrock). The switch between HBO and LED illumination was made using an internal motorized mirror controlled by Zen software.

#### 2.6.3. Coupling

No triggering connection is made between the AFM group (AFM head, AFM controller, AFM computer) and the optical group (optical microscope, camera and imaging computer).

#### 2.6.4. Noise and temperature control

The AFM and optical microscopes were isolated from ambient acoustic and mechanical noises using acoustic foam and an active damping table (Halcyonics). All experiments were carried out at 25 °C (except when mentioned), for no more than an hour and a half when cells were present, before replacement of the substrate, cells (if any) and cantilever.

### 2.7. Cantilever modification: glueing a bead

9.6 μm diameter latex beads (Invitrogen) were glued at the end of MLCT-UC levers using micro-manipulation techniques on a Biomembrane Force Probe/Micro-manipulation set-up [35]. Briefly, a diluted ultra pure water suspension was let to dry on a coverslide and an UV curing glue (OP29, Dymax) was spread close by. A cantilever (attached with double face tape onto a 3D micromanipulator (Sutter Instruments)) was first dipped into the glue, then approached from a bead under constant bright field microscopy observation. After lifting the bead from the surface, the glue

was allowed to pre-polymerize for $>5$ min under the direct light of the halogen lamp of the microscope set to its maximum power. Then the lever was collected and cured for 20 min in a UV oven at maximum power (BioForce Nanosciences). The presence and position of the bead was checked by microscopic observation of the lever at the end of the process, from a top view and from a side view, allowing a precise determination of its radius using Fiji software [42] (see Supplementary Fig. 1B). Note that the chosen glue does not introduce any large auto-fluorescent background as it has been observed with 2-component epoxy glues (the autofluorescence being slightly present in the B light, but not in the G or R ones, not shown). The rigidity of the bead/glue/lever link is far greater than the one of the tested cells as seen as a rigid, linear behaviour when calibrating the modified lever in situ on glass.

### 2.8. Mechanical characterization of the cells as a function of labelling

In order to measure the local Young modulus of the cells, AFM indentation experiments were performed using non modified MLCT-AU levers. Adhered cells were selected by optical examination and the pyramid shaped tip was positioned in the centre of the cell. Resulting Young moduli were found to depend neither on the fine positioning of the lever when indenting the central, higher part of the cells (excluding any lamellar, thinner structure that may exist at the border of the cell) nor for the use of MLCT levers with or without gold coating (not shown).

The maximal exerted force was set at 500 pN (leading to indentation depths of the order of 1 μm), the contact duration at 0 s, the speed of pressing and pulling at 2 μm/s in all cases. At least 10 force curves were recorded for each cell. Each force curve was examined visually and processed with the JPK DP software (JPK Instruments): corrections for baseline, possible tilt of the baseline and a modified Hertz model for pyramidal tips were applied (see above), making the hypothesis that the cell behaves as an incompressible material [37]. The entire force span (from the baseline to the maximal contact force) was fitted. A median value per cell was then calculated and tabulated, leading to the distribution for at least 13 cells in each condition, with or without the Fluo4 labelling. The resulting box-plots were then plotted using Matplotlib (http://matplotlib.org/) and Seaborn (http://stanford.edu/~mwaskom/software/seaborn/) Python libraries. No obvious correlation between the Young modulus and the force curve number (corresponding to the "mechanical history" of the cell) was observed and, during occasional longer ($>1$ s) contact times experiments, no large difference in relaxation patterns of different cell types was revealed (not shown).

### 2.9. Study of the coupling signal

Clean coverslides were mounted directly in the Biocell or CoverSlip Holder (JPK Instruments) and covered with 700 μL PBS $1\times$ w/o $Ca^{2+}/Mg^{2+}$. Unless indicated, the experiments were performed at room temperature.

After calibrating the desired lever and checking that its spring constant was consistent with the manufacturer's nominal value, the lever's end was set at a height of ~7.5 μm from the coverslip (Fig. 1A). This distance is comparable to the typical thickness of a T cell or a macrophage attached to a substrate (up to 10 μm). Focus was adjusted, in bright field, onto the lever end.

Using Zen software (Zeiss), the wavelength, power (in %), duration and interval (s) were chosen and sequences of light pulses (duration 0–500 ms, intervals 200 ms–several seconds) were flashed using the LED illumination system onto the lever. Simultaneous recording of the lever deflection was made at 1 kHz using the JPK SPM software Real-time option. Data was saved as text (.csv) files and processed using IgorPro (Wavemetrics) or Python 2.6 for measurements using built-in procedures or programmed ones. Final values were stored in LibreOffice Calc sheets. The resulting data graphs were then plotted using Matplotlib.

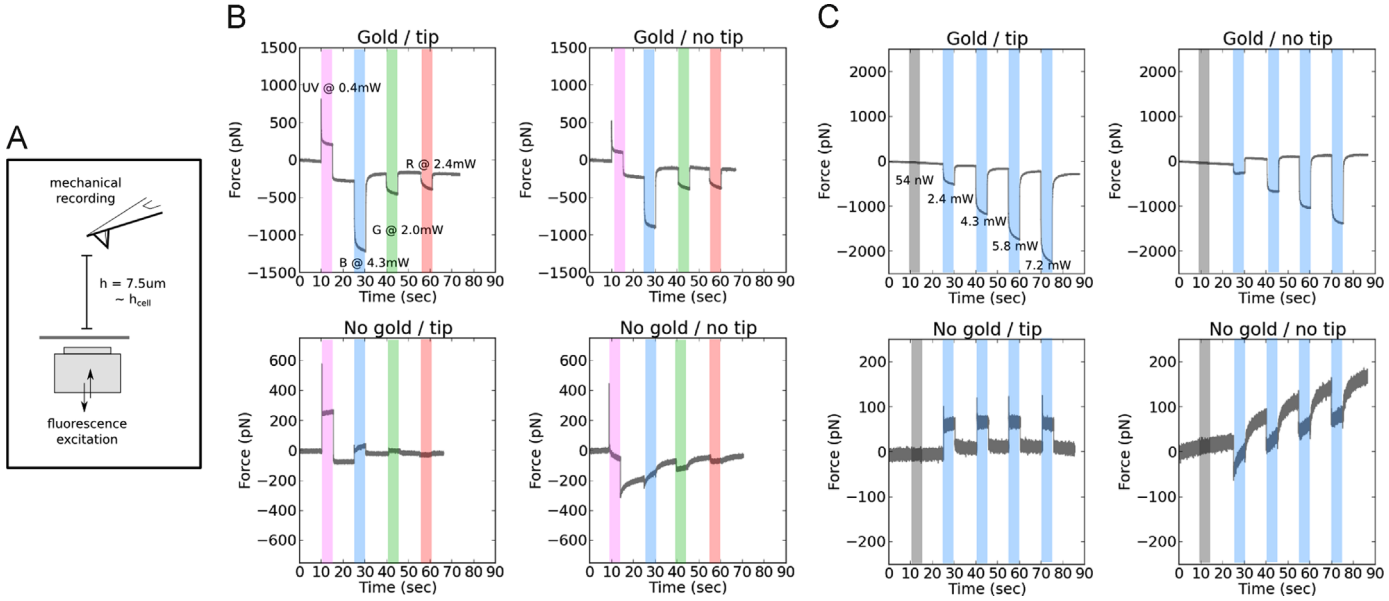


**Fig. 1.** Observation of the AFM/fluorescence coupling signal. 5 s fluorescence excitation was used at different wavelengths, with a MLCT large triangle lever with or without gold, with or without tip. (A) Schematics of the experiment. The cantilever end is set at a height of ~7.5 μm above the coverslip (see text). (B) The coupling signal shape and sign depend on the type of coating of the lever and on the wavelength of the excitation. These representative signals have been acquired at the half max power of each diode (UV (violet), B (blue), G (green) and R (red)), corresponding to the noted powers. (C) Signal intensity variation upon increasing the blue diode power (0%, 25%, 50%, 75% and 100% of diode power, corresponding to the indicated real measured power values). Levers with a gold coating show a strong dependence of the coupling signal at 470 nm excitation upon its power (grey stripe, off; blue stripes, on), whereas the non gold coated levers appears to be rather insensitive to this parameter. On (B) and (C), the relaxation for the levers with a gold coating to come back to its resting state appears to be slow, and drift is more important. (For interpretation of the references to colour in this figure legend, the reader is referred to the web version of this article.)

### 2.10. Light power measurements

The power of the excitation fluorescence light was measured using a PM100D power-meter (ThorLab) in combination with a S120C probe (ThorLab), directly at the exit of the objective. With the help of a paper sheet, the focusing of the lens of interest (40 × NA0.75 for force measurements or 20 × NA0.8 for light stimulation ones) was made using 470 nm visible diode (LED configuration B). Using the microscope stages, the *x*,*y* position of the detector was set so that the resulting measured power did not vary for any minute motion of the detector over the lens. Wavelengths and nominal power (LED illumination %) were varied using the remote control of the LED system (Zeiss), while the mean value and SD over an averaging period of 10 s were measured. No wavelength correction was applied to the signal detected.

### 2.11. Following the dynamics of the LED system emitted light

A high speed giga-ethernet camera (GE 680, Prosilica), attached to a computer independent of the AFM / fluorescence set-up, was used in combination with the JAI SDK and Control Tool (http://www.jai.com) to record the excitation light sequences emitted by the LED system. These sequences were imposed by the Zen software (Zeiss). A semi-reflective filter was used to redirect part of the light onto the fast camera set to a ROI size that allowed acquisition up to ~1000 fps. The exact frame rate was recorded by JAI SDK while taking the movie. The obtained movies were processed using Fiji to calculate the mean intensity of the images vs. time. The subsequent data was plotted and analysed using Matplotlib library for Python (see Supplementary Fig. 3A).

### 2.12. Mechanical stimulation of cells and recording of calcium fluxes

Adherent and Fluo4 loaded lymphocytes, or macrophages, were contacted with bead decorated levers under a max force of 1nN, with a pressing and pulling speeds of 1 μm/s for a total cantilever travel distance of up to 10 μm. Typical contact times were 180 s for lymphocytes and 120 s for macrophages. Fluorescence was simultaneously excited by 200 ms pulses of 50% LED in configuration B (~4.5 mW), separated by 2 s intervals.

Images were saved as .tiff files sequences and processed using Fiji software: the background, the cell submitted to the mechanical forces and eventually some surrounding cells were ROI-ed using the circle tool with zones of equal area, then the fluorescence level, *F*, (as grey levels) was measured. Ad-hoc Python or IgorPro procedures were then used to automatically (a) subtract the background, $F_0$, from the cell fluorescences frame per frame (b) calculate the ratio $F/F_0$ (c) post-synchronize the fluorescence ratio with the force as a function of time by aligning the first coupling signal to the first picture data. The synchronization of the other coupling signals/frame fluorescence signals was carefully inspected along the force vs. time curve. The resulting graphs were plotted using Matplotlib library for Python 2.6.

### 2.13. Mechanical recording of the effect of activating Rac–PA

Rac–PA transfected cells were selected by imaging them with B light at 100% for 250 ms using a 20 × NA 0.8 lens (~36.8 mW). After setting the lever above one cell, the sample was kept in dark for a couple of minutes i.e. far longer than the half life of the excited state [38].

#### 2.13.1. Before/after experiments

Up to 10 force curves were taken at 1 nN max force and 1 μm/s speed, with a gold coated lever with a pyramidal tip. Then, a 15 s light pulse was used to activate the protein by illuminating the entire field of view. Then, up to 10 additional force curves were taken subsequently, as soon as the fluorescent light was switched off. Using the same methodology as described above, we measured the Young modulus for each indentation curve. Median values, for each cell, before and after the pulse were calculated and plotted as a box-plots, for cells having been (or not) transfected with the plasmid and (or not) starved overnight.

#### 2.13.2. Real time experiments

A succession of force curves (max force 500 pN, speed 1 μm/s) were continuously taken using a lever without gold coating and with a pyramidal tip. The 15 s pulse was applied by illuminating the entire field of view. The force data were recorded in real-time at 1 kHz together with separate force curves (which were used to obtain the Young modulus). The post-synchronization of Young modulus vs. time was performed as follows: on the force vs. time plot, the coupling signal was observed and used, together with the position of the first maximum in force as obtained using Python. The position of the subsequent maxima was used to position the Young modulus values versus time. Note that the separation in time is not homogeneous because it depends on the local value of *E* (the smallest the *E*, the longer the time to reach the max force will be) if one indexes the max value of indenting force to the image time stamp.

### 2.14. Statistics

Data processing was performed using open source softwares on Linux PC machines. Linear fitting was performed using QtiPlot (http://www.qtiplot.com/) software and cross-checked using Statsmodel library for Python 2.6, and Calc from LibreOffice 3.5. Box-plots were plotted using Python Seaborn library using Spyder2, and cross-checked with classical Python Matplotlib and R procedures. Data were processed using R/Rstudio softwares for statistical analysis using existing packages (http://cran.rstudio.com/, packages asbio and pgirmess for Kruskal–Wallis or Wilcoxon tests).

## 3. Results

### 3.1. The fluorescence excitation light causes the AFM lever to bend

As reported qualitatively in the AFM community (see Section 4), a coupling signal is observed between cantilever deflection and fluorescence illumination (Fig. 1). Here, the use of a diode illumination system allowed to vary systematically the wavelength, power, duration and intervals of the light pulses. Since neither a shutter is used nor a mechanically moving piece attached to the optical microscope, on which this AFM stands, such an illumination system has no direct mechanical impact on the entire set-up: as a control, the system was set on/off for a controlled duration with a diode power of 0 W, and no signal was seen (Fig. 1C, shaded zones). The characteristic time for the diodes to reach their plateau emission for a given power is $<1$ ms (data from provider and Supplementary Fig. 3A), much lower than the typical illumination durations that are used for regular fluorescent compounds typically used in biology to get good *S*/*N* ratios ($\sim$100 ms).

The coupling signal was verified to be reproducible (Fig. 2A, Supplementary Figs. 3 and 4); its shape (for visible excitation wavelengths) and magnitude varied strongly as a function of the presence or absence of a layer of reflective gold on the backside of the cantilever (Fig. 1B). The magnitude varied strongly upon the power of the excitation light at a given wavelength when the lever was coated with gold, and showed very little, if no, variation when no gold layer was present (Fig. 1B, C, Supplementary Fig. 2). For a

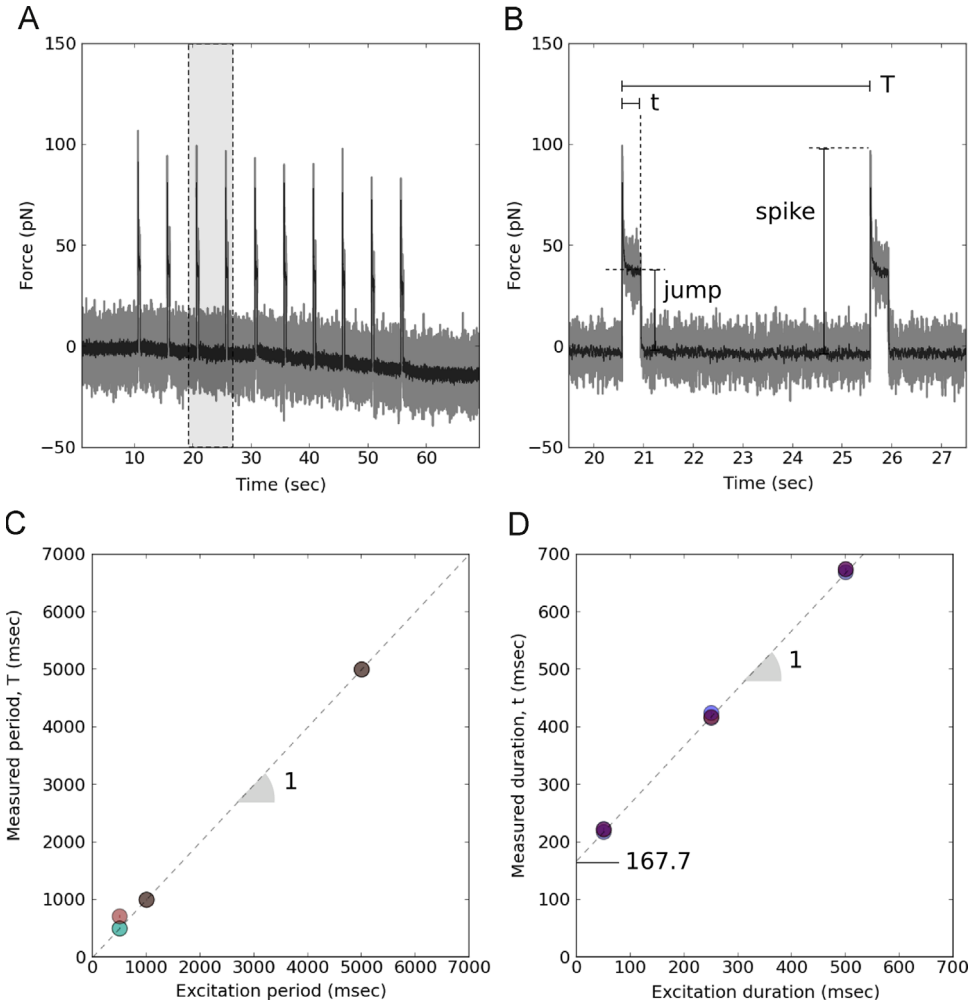


**Fig. 2.** Using the coupling signal as a timer. Characterization of the coupling signal observed at 470 nm. (A) Typical repetitions of short pulses (50 ms every 5 s) of excitation light as recorded by the deflection of the lever for MLCT-UC large triangle lever. (B) zoom, corresponding to the grey zone in (A), on two successive signals detailing the shape of the signal. *T* is the period and *t* the duration of the response of the lever to the light pulse. (C) Period of the observed lever bending, *T*, as a function of the imposed excitation period. The SD of the measurements (over at least 10 measurements) are smaller than the marker size. Combinations of imposed durations (50, 250, 500 ms) and imposed periods (500, 1000, 5000 ms) are represented as points of different colours (red, blue, green, as a function of the value of duration) that collapse as black dots except for the case of $t=T=500$ ms (red dot). The dotted line is a slope/linear fit of slope 1.0 with a $R^2=0.99$. (D) Duration of the observed lever bending, *t*, as a function of the imposed excitation duration. Combinations of $t=50$, 250, 500 ms and $T=500$, 1000, 5000 ms are represented as points of different colours (as a function of the value of *T*). The SD of the measurements (over at least 10 measurements) are smaller than the marker size. The dotted line is a linear fit of slope 1.0 and intercept 167.7 ms with a $R^2=0.99$. (For interpretation of the references to colour in this figure legend, the reader is referred to the web version of this article.)

given lever type, the shape and sign (i.e. positive or negative forces) appeared to be dependent on the wavelength (Fig. 1A, in particular when comparing visible vs. UV lights, and Supplementary Fig. 2). The relaxation of the lever was slow when gold was present and rapid otherwise (Fig. 1C). The presence of a glued bead of 10 μm in diameter, or its type (polystyrene or glass) did not modify largely the shapes and magnitudes of the observed signal (for G light, see Supplementary Fig. 6F, G; for other wavelengths, the results were similar, not shown). We did not vary systematically the size of the bead, but from our results one may infer that beads up to 10 μm in diameter do not strongly affect the signal, regardless of their composition. This is also supported by the fact that the effect of the presence of the tip was rather negligible under our experimental conditions, in regard to chemical treatment or presence of gold (Supplementary Fig. 2). Aside, (i) the absolute deflections were very large for UV light for all cantilever types and for visible light when gold coating was present (e.g. for commercial levers, $\sim -2000$ pN with gold vs. $\sim +50$ pN without gold for 470 nm excitation at maximal diode power) and (ii) the AFM showed a higher stability in time (i.e. smaller baseline variation) when using gold-less cantilevers (Fig. 1).

The main effect of the absence of gold coating was to abolish the variation of the shape and intensity of the coupling signal as a function of the excitation power for visible wavelengths, and to keep the observed deflection at low forces in particular for the 470 nm excitation (Fig. 1C). This wavelength corresponds to the excitation of calcium reporter molecules of the Fluo4 family that were of particular interest for the present study. As a consequence, we set out to characterize the step-like coupling signal observed with commercially available MLCT-UC levers (having a tip but no gold coating), in order to use it as a timer signal. Such levers have the advantage of not suffering from harsh acidic treatment that may damage them or be imperfect (Supplementary Fig. 1A).

By inserting an IR filter in the AFM head (780 nm, diameter 12.5 mm, Edmund optics, maintained on the JPK glass block using immersion oil), it was verified that the observed signal was not created by an incoming light from the visible diodes onto the QPD (not shown). Using AFM force mode in either constant height or constant force mode during the contact with a hard glass substrate, it was concluded that the signal resulted from an actual bending (potentially with complex modes of deformation) of the lever by observing its decrease or disparition (Supplementary

Fig. 4). Moreover, the signal did not appear to vary (for gold less levers) when the cantilever travelled towards or away from the substrate over several micrometres, at various speeds.

The magnification (10×, 20×, 40×) and the NA of the lens (air 40× NA0.5, air 40× NA0.75, oil 40× NA1.20) were varied and the coupling signal was observed in all cases, with variable intensity but qualitative identical behaviour/shape (not shown). We then chose for the rest of the study the 40× NA0.75 air lens since it represented a good compromise between working distance, magnification and sensitivity for fluorescence measurements for our cell types. Moreover, this air lens does not introduce any supplementary mechanical coupling between the AFM and the optical microscope.

### 3.2. Using the coupling signal as a timer

We studied the characteristics of the coupling signal observed in the case of a commercial MLCT-UC lever (Fig. 1C, magnified in Fig. 2) in order to determine how to use it to synchronize the AFM force signal and the fluorescence imaging. The coupling signal is composed of a rapid, almost instantaneous, spike, followed by a rectangular jump. We submitted a large triangle lever to periodic illumination of B light of controlled duration and period and quantified the effect in terms of time (duration, *t*, and periodicity, *T*, Fig. 2) and magnitude (amplitude, in force) (Fig. 3). Keeping the medium at room temperature (~20 °C) or imposing the temperature to be 25 or 37 °C using a temperature control system (Biocell, JPK Instruments) did not change the observations reported below (not shown).

The period, *T*, varied linearly, as expected, with the imposed illumination period, with a slope of 1.0 (Fig. 2E). Combinations of imposed durations (50, 250, 500 ms) and imposed periods (500, 1000, 5000 ms) are represented as points of different colours (as a function of the value of duration). They collapse as black dots except for the case of duration=period=500 ms (red dot). A first conclusion is that the coupling signal could then be used reliably as a timer.

The duration of the lever deflection, *t*, was measured as a function of the imposed excitation duration (set via Zen software), on the same lever, with the same combination of duration/period (coded in colours in Fig. 2D). A linear response is achieved with a slope=1.0 but with an intercept of 167.7 ms, showing that the recorded response of the lever is longer than the desired excitation. We found this extra duration to originate from the [camera (firewire)/diode illumination system (USB2)/acquisition software] part of the set-up, and could not be decreased very notably by playing either on the ROI of the acquisition or on the camera binning (Supplementary Fig. 3). This introduces a limitation on the shorter excitation/shorter periods that can be used with our system.

We further examined the force characteristics of the coupling signal on three of the softest levers commonly used in biology: MLCT-UC 10 pN/nm (large, triangle), 20 pN/nm (rectangle), 30 pN/nm (small, triangle) (Supplementary Fig. 1A). While the rectangular jump height did not appear to depend on the excitation power at 470 nm (Fig. 3A), the spike seemed to be more variable for a given power (higher SD) and for varying powers (Supplementary Fig. 3A). The shape of the lever appeared to have a rather strong influence on the spike height (Fig. 3B) and only a moderate one on the jump height (Fig. 3C). It is noteworthy that the two signals were always >5× and ~2× (respectively) higher than the typical noise of our AFM (~15 pN). As a consequence, this signal could be always seen and, as long as forces that are used / measured are on the 500–1000 pN range, would be only a moderate modulation of them. Interestingly, the large triangular and the rectangular levers appear to have to the smaller signals of all.

In order to extend the use of this signal as a timer, we examined the use of two wavelengths, either consecutively of simultaneously, and confirmed that the use of gold-less cantilevers can be efficiently extended to such a situation with similar precautions and restrictions (Supplementary Fig. 5). This leads to envision the use of this system for dual stimulation dyes or combinations of dyes for ratiometric measurements (e.g. Fluo4/Fura-Red), in combination with a vibration free, single camera, dual-detection using e.g. a DualView (DV2, Photometrics) system (see Section 4).

As a conclusion, the observed coupling signal for gold-less levers could be efficiently used as a way to synchronize the fluorescence images and forces in a mechanical stimulation experiment, whilst perturbing very moderately the applied or measured forces.

### 3.3. Immobilisation of immune cells and activability

We selected PLL as a relatively non-activating but efficient binding molecule for Jurkat T cells [9]. To verify cell activability, we used 10 μM ionomycin in DMSO to stimulate adherent Fluo4 loaded cells. The max $F/F_0$ ratio was observed to be ~6.2 for

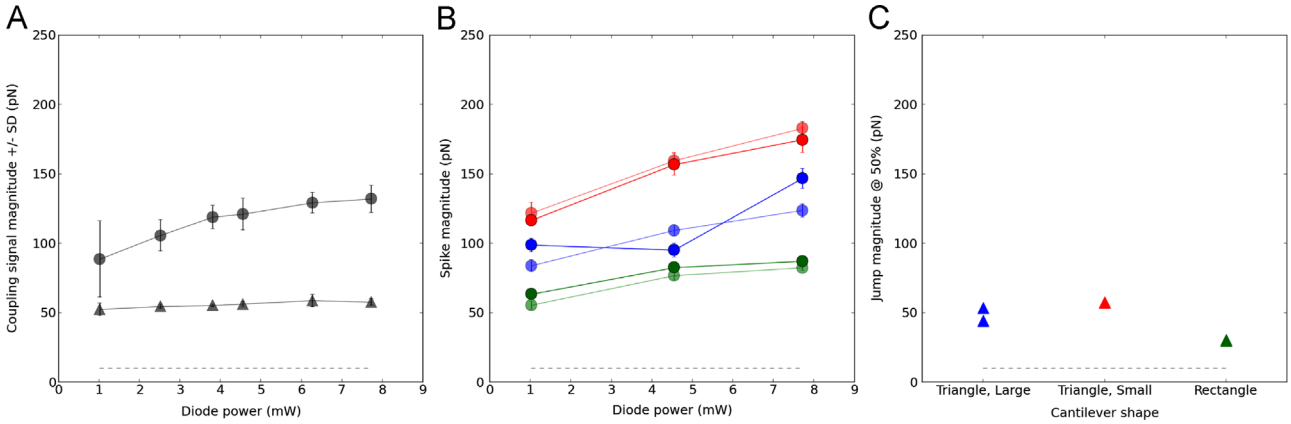


**Fig. 3.** Effect of lever shape and spring constant on the coupling signal. (A) Influence of the excitation power upon the spike (circles) and jump (triangles) magnitudes for a MLCT-UC large triangular lever. The jump appears rather independent of the power, smaller that the spike signal by at least a factor of 2, and the two signals are always larger than the typical noise of the experiments. (B) Influence of the power on the spike intensity (which shape does not vary) for two MLCT-UC cantilevers sets, showing the chip-to-chip variability (with $k$=11.8–17.44, 38.9–38.7, 18.2–21.9 pN/nm respectively for large triangular (blue), small triangular (red) and rectangular levers (green)). (C) Same levers as in (B), but for the magnitude of the jump (same colour coding as in (B)). The presented data was gathered using an excitation power of 4.3 mW and $t$=200 ms. (For interpretation of the references to colour in this figure legend, the reader is referred to the web version of this article.)

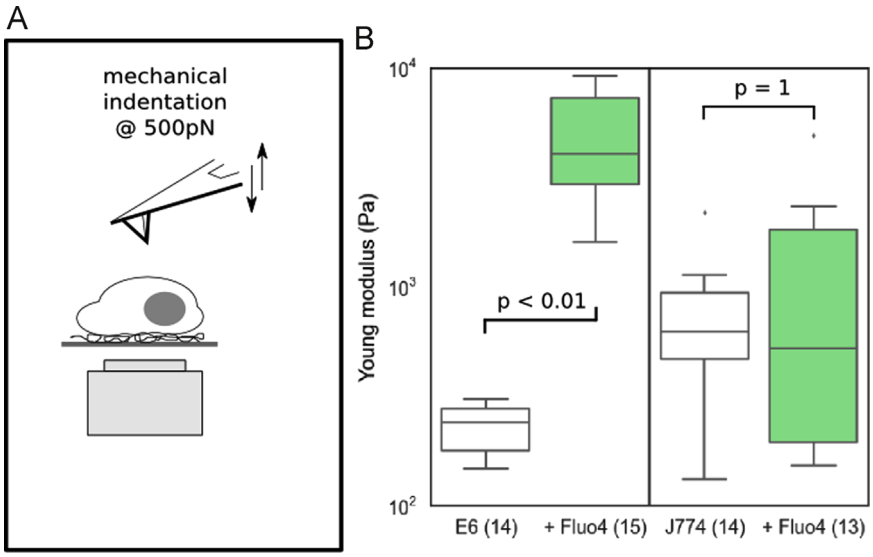


**Fig. 4.** Mechanical characterization of PLL adhered lymphocytes and adhered macrophages using a pyramidal indenter. (A) Schematics of the experiment. (B) Young modulus (log scale) as a function of cell type (left panel, Jurkat T cells; right panel, J774 macrophages) and labelling with calcium reporter (white boxes, no dye; green boxes, with Fluo4). The number of tested cells are indicated for each conditions. (For interpretation of the references to colour in this figure legend, the reader is referred to the web version of this article.)

populations of Jurkat E6.1 cells (as compared to 2.6 when DMSO alone was used). For untreated glass adhered J774 macrophages, we found this ratio to be ~5.2 (as compared to 2.6). Experiments were performed at room temperature to avoid excessive sequestration of the Fluo4 dye in organelles. Using soluble activating anti CD3 antibodies leaded to calcium fluxes in Jurkat cells, with lower maximal ratio in comparison to ionomycin (not shown).

### 3.4. *Quantification of cell mechanics as a function of cell type and Fluo4 loading*

Using the pyramidal tip of soft gold coated levers, the mechanics of immobilized model lymphocytes and macrophages was investigated. Their Young modulus, *E,* was measured over the entire indentation range, using a given max contact force (500 pN) and at a given speed (2 μm/s) (Fig. 4). We found *E* values in the range of 100–1000 Pa, coherent with the values found in the literature for various types of white blood cells [9,43,44]. These values did not vary largely, for the Jurkat cells, when the temperature was 25 °C or 37 °C, or when the speed used for pressing the tip on the cell was varied between 1 and 10 μm/s (not shown), indicating a weak contribution of cytosol viscosity in this range of stimulation frequencies. The basal mechanics of the two cell lines was similar for the populations tested, the macrophages being slightly more rigid than the T cells (which is consistent with Ref. [45]). For the macrophage line, the labelling with Fluo4 did not exhibited a marked difference to the basal level. Interestingly, the Jurkat cell line exhibited a significant variation of its Young modulus: the cells were more rigid when loaded with Fluo4 with no supplementary modification of the cells environment (Fig. 4).

### 3.5. *Mechanical stimulation of a single cell*

The coupling signal was used as a way to synchronize a micromechanical stimulation of a single cell and the simultaneous recording of intracellular calcium fluxes. Experiments were performed, at 25 °C, by pressing a bare latex bead, glued to the large triangle of MLCT-UC (no gold, nominal constant 10 pN/nm) onto adhered, Fluo4 loaded cells, while having set the focus for the optical detection onto the equator of the cell. Two prototype patterns that recapitulate the essential steps observed for the cells exhibiting visible calcium fluxes are presented in Fig. 5.

Upon reaching a pre-set maximal contact force of 1 nN (Fig. 5D #3, E #2), the piezo motion was stopped using closed-loop system, for a purely mechanical, continuous, stimulation. The cell could relax the stress via its viscoelastic properties (Fig. 5D #4, E #3) [46] and even apply pulling (negative variations) or pushing (positive variations) forces to the stimulating bead (Fig. 5D #4–5, E #4–5) [31].

For model T cells, when observed, the calcium signal was showing a single peak, delayed from the force peak, here ~30 s apart (Fig. 5D). The calcium peak was often observed to synchronize with some active behaviour of the cell (Fig. 5D, after #4), as monitored by modulations of the force levels achieved after the partial relaxation of the contact force. Surrounding, non mechanically stimulated cells were neither showing such a calcium peak, nor fluctuations (Fig. 5D, control). The observed fluorescence signal eventually plateaued and quickly decreased with different intensity vs. time slopes (slow then fast, then slow), potentially due to the combined effects of the return of the cell to its basal calcium level and/or the Fluo4 bleaching. When the bead was finally pulled from the cell surface, non specific adhesion was recorded (Fig. 5D #5), but total separation was possible for the accessible piezo pulling range (Fig. 5D #6), the cell staying attached firmly onto the PLL, with no apparent damage as observed in transmission microscopy. Sometimes tethers that were pulled from the cell and not fully detached at the end of all processes were observed (not shown).

For model macrophages, the pattern of fluorescence was observed to be more complex, often exhibiting oscillations in response to mechanical stimulation (Fig. 5E). The fluorescence fluctuations did not seem to be correlated with force fluctuations (Fig. 5E #3). The most prominent differences with the T cells appeared during the relaxation phase, where negative forces were recorded, meaning that the cell pulled on the bead (Fig. 5E #4), and during the separation process where the recorded adhesion forces were exceeding the detectable bending capabilities of the lever/QPD system (Fig. 5E #5). When moving away the lever from the surface by using AFM head motors and introducing a lateral motion of the head, the macrophage was always found to have detached from the substrate and to be bound to the bead, indicating that a potential phagocytosis event was at play [47].

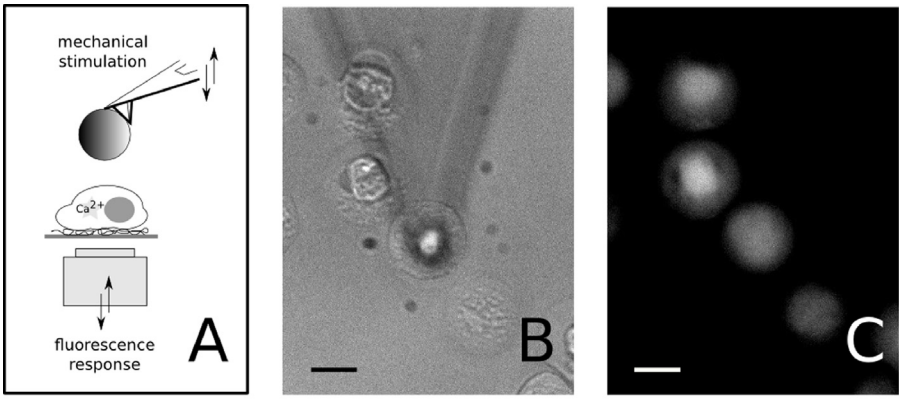
mechanical stimulation
Ca2+
fluorescence response
A
B
C

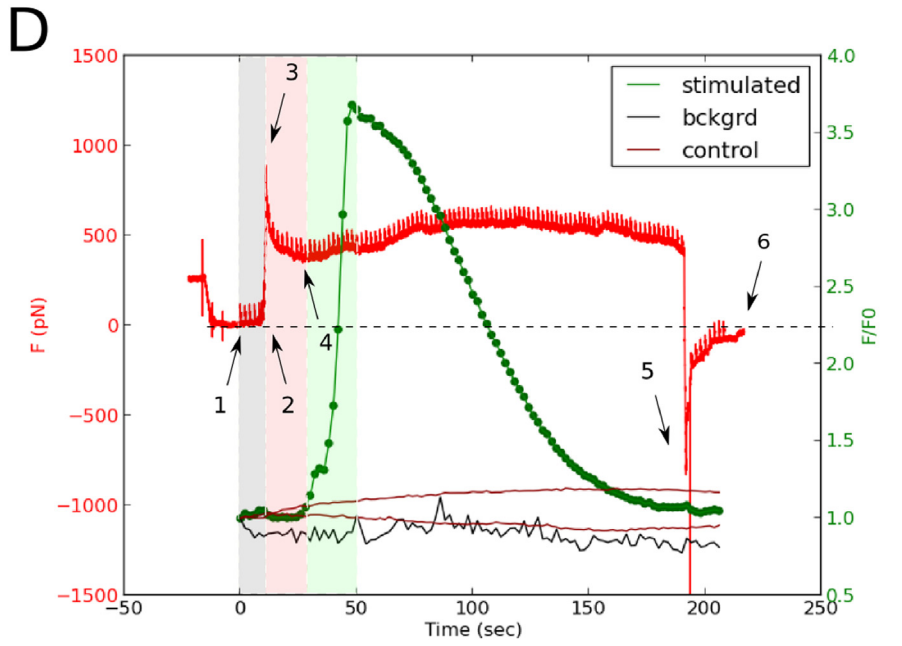
D
stimulated
bckgrd
control
F (pN)
F/F0
Time (sec)
1
2
3
4
5
6

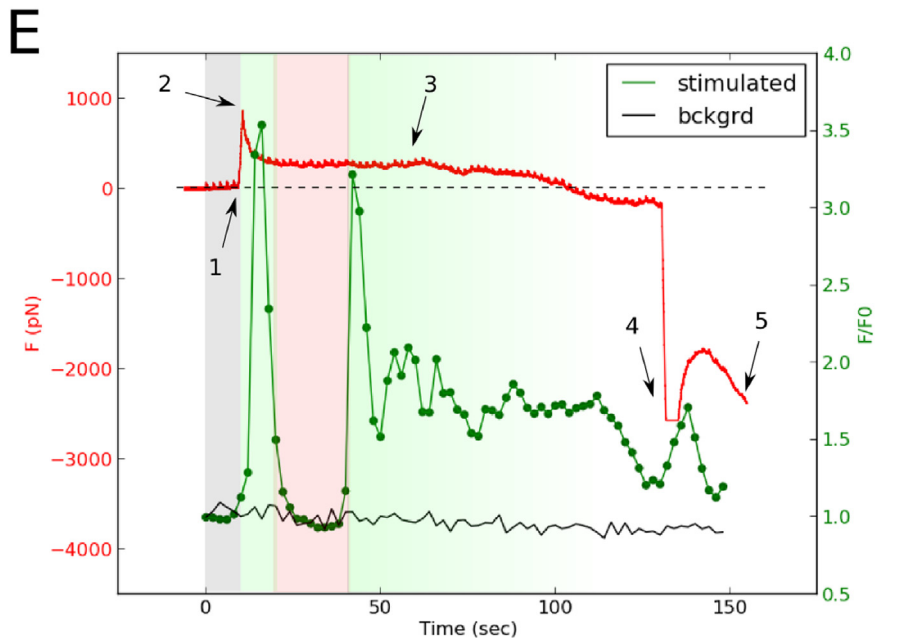
E
stimulated
bckgrd
F (pN)
F/F0
Time (sec)
1
2
3
4
5

### 3.6. Mechanical recording of Rac activation in Jurkat cells

A reciprocal approach to the previous experiments consisted in using the coupling signal between fluorescence and AFM force mode to follow the real-time mechanical modifications of photoactivable Rac transfected Jurkat cells.

First, mechanical characteristics of cells upon activation of Rac were examined at a population scale, with a "static" approach, by measuring the elastic modulus before and after an activating light pulse, using unmodified MLCT-UC levers. Median values, for each cell, before and after the pulse were calculated and plotted together with descriptive parameters of cell population as box-plots, for cells having been (or not) transfected and (or not) starved overnight, in combination (Fig. 6A–D). Comparison of the median of the cell population did not show the existence of a strong effect, but the close examination of the behaviour of individual cells (using the connecting lines on Fig. 6A–D) showed that, when Rac–PA was present and activated, more tested cells were showing an increase in their rigidity. This was confirmed by the examen of the fraction of cells exhibiting an increase in $E$ over the activation of Rac–PA (i.e. having a median $E$ after light pulse to median E before ratio greater than 1), for the different cell conditions (Fig. 6E). This effect appears to be mainly due to the action of Rac–PA (see Fig. 6A vs. C, Fig. 6B vs. D, and E) rather than to starvation (see Fig. 6A vs. B, Fig. 6C vs. D, and E). Aside, the spreading of the distribution before and after the light pulse did not appear to be different, indicating that cell populations mechanical heterogeneity was not affected. Interestingly, the starved cells appeared to be significantly stiffer than the non starved ones. In an other set of experiments (to be reported elsewhere), the transfection protocol of Jurkat with various plasmids was observed not to largely modify Young modulus values obtained under moderate indentation forces (500–1000 pN).

In order to dissect the behaviour of individual cells, preliminary experiments were performed to follow in real-time the Young modulus of a given cell, using a MLCT-UC large triangle lever, when stimulating the cell with 470 nm intense light ($\sim$37 mW for 20$\times$ NA0.8). Starved Rac–PA transfected cells were used since they appeared previously to have a strong response to the stimulation (Fig. 6E). The coupling signal was used here to detect the beginning of the stimulation period in the real-time recording of the force, hence to place the measured values of $E$ vs. Time and the stimulation duration, as exemplified on Fig. 6F–H. This allowed to observe that (i) the effect of the activating light was almost immediate, (ii) reached a plateau after the pulse was stopped and (iii) rapidly decayed ($<$45 s duration, which is consistent with published data [38]). The values before and after the pulse were similar, and some cells exhibited a strong variation of $E$ upon stimulation, as could also be observed in individual median signals from Fig. 6D. The rapid and transient, reversible nature of the light induced perturbation may lead to an apparent weaker effect when calculating a median over time in the regions before and after the activating light pulse in the previous experiments. As a conclusion, the presented AFM/fluorescence coupling effect allowed to directly, and in real-time, observe modulations of the cell mechanics upon light activation of Rac that the simple examination of population behaviours may have not allowed to detect.

## 4. Discussion

A deflection signal that appears when usual wavelengths of fluorescence excitation light are shone onto a soft AFM lever has been observed and described. This coupling signal varies (i) in shape as a function of the presence of a reflective gold layer and as a function of the wavelength used, and (ii) in intensity as a function of the power of the light when a gold coating is present. However, this signal appeared to be, in the absence of gold reflective coating, regular and of small amplitude ($\sim$50–100 pN), with the same period as the imposed excitation, and with a controlled duration that varies with the duration of the excitation. It was concluded from controls that this signal cannot be totally removed, but minimized by using the proper type of commercially available AFM levers.

Importantly, it must be noted that this coupling effect has been observed qualitatively among several labs, with different brands/types of AFM, and with light sources such as halogen lamps, diodes or lasers (C.M. Franz, F. Rico, A. Rigato, F. Eghiaian, personal communications, among others), but it has not been fully described and, to our knowledge, never exploited as we propose here.

As a consequence, we chose to use it to synchronize the signals coming from the AFM (force) and from the fluorescence detection (image) with no additional electronics, in mechanical stimulation experiments where the cellular consequences activation was followed by simultaneous fluorescence measurements. Conditions for this usage as a timer were established in time ranges that are compatible with the use of single wavelength calcium probes such as Fluo4 to have (i) sufficient excitation for a good detection and (ii) minimize dye bleaching.

Subsequently, this signal was used to follow, in real time, calcium response of T cells and macrophages when submitted to a purely mechanical stimulation to demonstrate the capabilities of the AFM/fluorescence set-up and the richness of the accessible mechanical, adhesive and signalling information. Single cell passive (elastic deformation and viscous dissipation) and active behaviours (pushing/pulling) were recorded with an excellent control over forces and times.

We also used the coupling signal in a reverse way, in order to record mechanical perturbations of single T cells when cytoskeletal modifications were induced by the use of a photoactivable Rac. It was observed that the protein modified the mechanics by stiffening the cell. Single cell recording allowed us to observe delays and relaxations that might be due to the reversible

**Fig. 5.** Mechanical stimulation of adhered cells while monitoring internal calcium fluxes with Fluo 4 dye. We used MLCT-UC large triangle with a bare 9.6 μm latex bead glued in front of the tip (see Supplementary Fig. 2). (A) Principle of the experiment, where a bare bead is approached from a cell at a given speed and pressed up to a force of $\sim$1 nN. At that moment, the position of the piezo is maintained constant, and the cell adapts and reacts to the applied force. (B) Transmission micrograph of the experiment, where the bead has been placed upon the centre of a FLuo4 loaded cell. (C) Corresponding fluorescence image. Bars: 10 μm. (D) Result of a stimulation on a PLL adhered Jurkat T cell (continuous contact of 180 s), after synchronizing the first picture (green point, 1) with the first spike of the coupling signal on the force curve (red line). Forces and fluorescence are represented versus time. The fluorescence (green dots) is corrected from the background signal frame to frame using Fiji plugins, and normalized to the first image ($F/F_0$). (1) first image; (2) cell/bead contact; (3) reaching maximal contact force, followed by cell viscoelastic relaxation; (4) when the cell starts pushing on the bead i.e. the force increases, the calcium signal appears significantly. Afterwards, the cell pushes/pulls on the bead as the modulation of the recorded forces shows. (5) When pulling, the cell appears to adhere to the latex bead but can be completely separated from it as the force goes back to the baseline. We observed that shorter continuous contact times (typically up to 20 s) did not produce such calcium rises. (E) same as (D), but with a J774 macrophage (continuous contact of 120 s). (1) bead/cell contact; (2) reaching maximal contact force before viscous relaxation; (3) force oscillations when calcium signal oscillate; (4) when pulling the bead away, the cell strongly adhere to it and eventually is released, in (5), from the surface. This could be a signature of a phagocytic-like behaviour. In (D) and (E), grey stripes are zones where the piezo moves, before the bead to cell contact. After the contact, red stripes are denoting low calcium levels, whereas rising or high calcium regimes are in green. (For interpretation of the references to colour in this figure legend, the reader is referred to the web version of this article.).

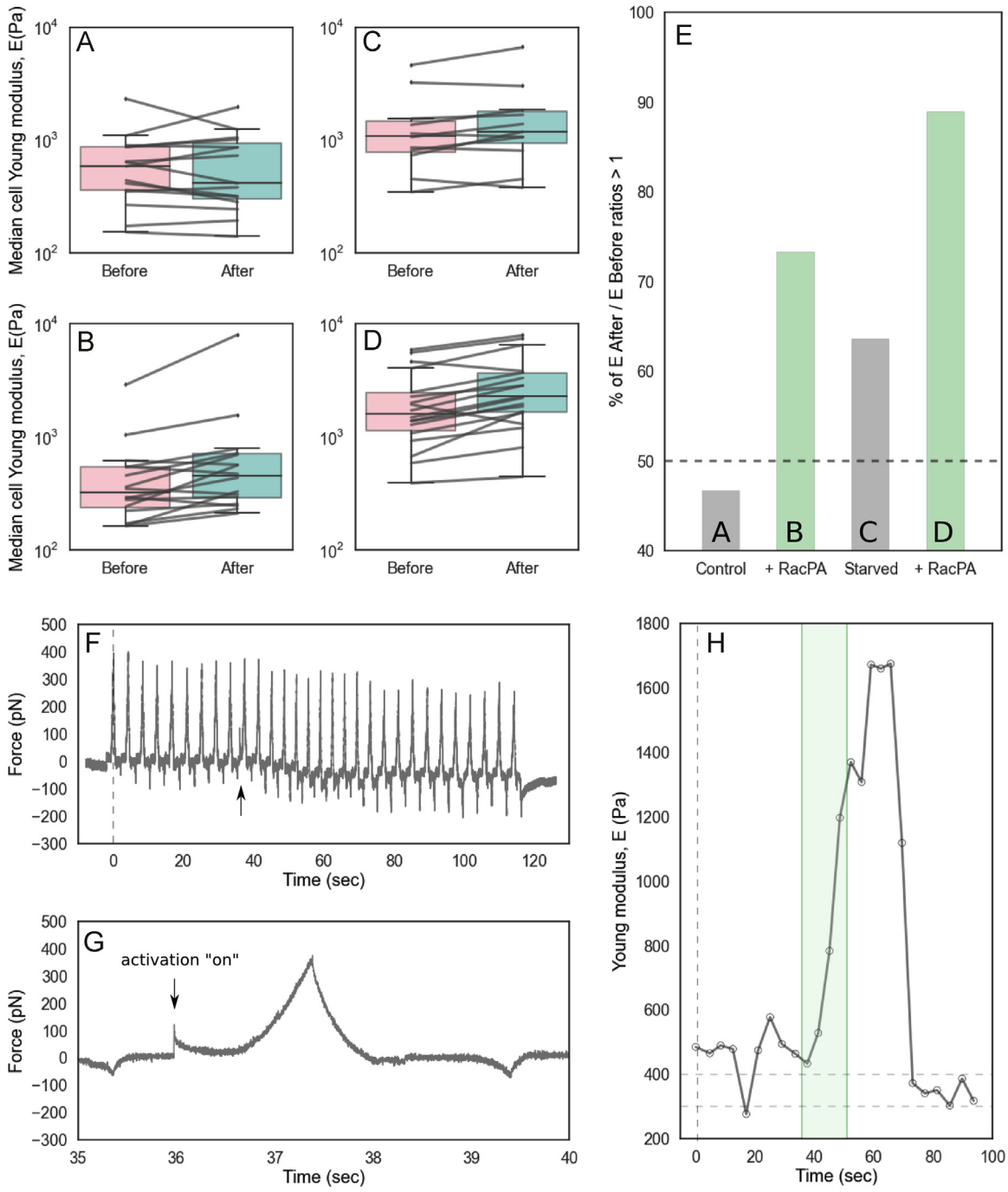


**Fig. 6.** Recording of mechanical response to light stimulation of Rac–PA transfected T cells. We indented the cells with large triangle levers with tip, with (A–E, MLCT-AU) or without gold (F–H, MLCT-UC). (A–D) Median Young modulus of cells distributions before and after 15 s pulse of blue light at ~36.8 mW (Colibri, 20× NA0.8) (A) non-transfected and non-starved, (B) non-transfected and starved, (C) transfected and non-starved, (D) transfected and starved cells. Each point is a median over up to 10 force curves for one cell for each condition. Box-plots of the populations, showing that no net difference of the median values over the populations (Wilcoxon $p=0.85$ (A), 0.65 (B), 0.22 (C), 0.20 (D)). Tendencies for single cells to present an increase in rigidity when Rac–PA is present, are superimposed as dots connected by lines. (E) % of $E$ after/$E$ before $>1$ as a way to quantify the previously observed tendency. (F) Prototypical real-time of force application on a transfected, starved cell. (G) Zoom on the zone where the starting of the activation light at 470 nm can be detected (arrow on (F), (G)). (H) Variation of the Young modulus over the first 100 s (from (F)) as a response of a 15 s pulse of blue light at ~36.8 mW (green zone), showing the absence of delay, the duration and the rapid relaxation of the effect. (For interpretation of the references to colour in this figure legend, the reader is referred to the web version of this article.).

photoconversion of the Rac variant among other potential causes.

Hereafter, open questions concerning the origin of this signal and limitations of its use that remain to be addressed are discussed.

### 4.1. Origin of the coupling signal

Controls were performed to clarify the origin of the observed coupling signal: (i) cantilever rigidity, shape, coating were tested; (ii) light intensity, wavelength were varied (the use of a mercury

lamp of 100 W provided qualitatively the same results as the ones shown here with the Colibri diode system); (iii) an IR filter was introduced in the AFM head to block any non-IR light that may have reached the QPD; (iv) temperature of the experimental buffer was not externally controlled (room temperature ~20 °C) or imposed at 25 or 37 °C in order to control the potential heating of the lever/medium by the IR laser.

It could be concluded that the signal is due to an actual bending of the lever (Supplementary Fig. 4). Low intensity fluorescence diodes, in liquid, may create a local heating of the lever, resulting in a bending since it is behaving as a bi component/bimetallic material. Commercial levers are usually coated on one side with chromium (or titanium), and in some cases with a supplementary layer of gold. When gold is present, the metallic layer deposited on the lever is thicker, so the lever is more asymmetric and possesses a more thermally conductive structure which may explain the larger effect that are observed on such levers (Fig. 1). The lever could then be understood as a local thermometer, and gold dilatation to create ample asymmetric motion of the lever, by bending it down (to negative forces).

On our set-up, the duration of the apparent effect has been shown to be biased by a residual time introduced by the fluorescence microscopy controlling system (Zen/Colibri/Camera), and could be slightly lowered (reduction ~10–20%) by using binning and ROI-ing the image (Supplementary Fig. 3). Nevertheless, this delay was never eliminated in our hands, hence reducing the time resolution accessible.

### 4.2. Modification of levers

When gold coating was absent or removed, we observed (i) that the levers were more "transparent" when observed in transmission (Supplementary Fig. 1), (ii) a subsequent decrease of the sum signal of the AFM (i.e. the total reflected laser reaching the QPD), similar for absent or removed gold cases, and that (iii) in the four conditions examined, the spring constant of corresponding levers was not varying much and that the variation stayed within the observed variation between cantilevers batches.

As reported by other groups [48,49], removing gold or using gold-less levers also improved the stability of the system: the drift was reduced to almost nil (Fig. 3A). A gold-less lever offered the supplementary advantage that the placement of the tip or the glued bead onto the cell and its centring were greatly eased. On another hand, this transparency implies to verify that the IR laser used for monitoring the lever bending has no strong influence on the cell's behaviour, as sometimes reported for optical tweezers (see below).

Removing gold with harsh acidic treatment was tested here but has shown some limitations: it was difficult to robustly achieve a very homogeneous uncoating along the entire body of the levers. In Supplementary Fig. 1, zones with different contrasts can be observed, suggesting an incomplete removal of the metal layer(s). Since the acidic treatment is vigorous, the underlying attaching layer of chromium (or titanium), or even the body of the lever itself, could be deteriorated non homogeneously. This could explain the differences between commercially available levers with no gold and chemically attacked ones in particular in the shape of the coupling signal, its sign and in its relaxation dynamics. Additional XPS studies of this residual layer may help to understand better the variation of the signal by allowing a refined description of the lever surface composition.

The cantilever tip, when present, limits the size of beads that could be glued on the lever end to obtain smoother, spherical indentors for mechanical stimulation (Supplementary Fig. 1B). In order to keep the benefit of the very regular signal that was obtained using commercially available gold-less levers, a new strategy (inspired by [50]), was preliminary tested on used levers, first washed with EtOH/ultra pure water, then air dried. A ion-beam milling set-up, coupled to a SEM, was used to cut the extremity of the lever to remove the tip without changing too much the lever length and their spring constant (Supplementary Fig. 6). In this way, the surface state of commercially available uncoated levers could be largely preserved together with their low spring constant. However, this technique is delicate and time consuming (1 lever per 20–30 min). We observed that the coupling signal for 470 nm exciting light is similar between a cut and a non cut levers (Supplementary Fig. 4D, E). The variations are of the same order as the inter lever dispersion observed (Fig. 3). The tip does not appear to contribute largely to the observed effect (Fig. 1, Supplementary Figs. 2 and 6). The same results were observed for levers without gold coating, bearing or not a 10 μm glass bead, supporting the fact that the bead does not affect much the observed signal, either in shape or in magnitude, in our optimized conditions (Supplementary Fig. 6F, G).

### 4.3. Lever mirror effects

Reports have shown that gold coated levers may act, when used in combination with fluorescence, as mirrors [33]. We set to observe this potential effect with non gold coated levers by measuring the fluorescence signal at different $(x,y)$ positions under the lever when pressing/pulling on a cell that did not present a strong mechanical activation (e.g. If contact time is kept low, ~10–20 s; Supplementary Fig. 7). In such conditions, the mirror effect was observed to be of rather low intensity, depended on the initial fluorescent level of the cell under study, and potentially of its spreading state (i.e. its thickness). When compared to the activation signal that were observed in Fig. 5D, E, this mirror effect is of small amplitude.

### 4.4. Precautions and further developments

#### 4.4.1. Limits of the timer

In order to be properly used, the coupling signal has to be characterized for every type of lever that could be of interest. The present article reports the use of gold-less, commercial silicium nitride levers that appear to have a reproducible, fast appearing/disappearing coupling signal, in particular when a blue excitation light is used e.g. for calcium reporters. In our hands, the main limitation is due to the existence of a ~160 ms extra duration of the coupling signal compared to the excitation coming from the excitation system, that, on our simple system, limits the possibility to take pictures at a high frame rate (i.e. with periods shorter than this extra duration plus the duration of the excitation). Aside, when using the coupling signal as a timer, the question of where to set the correspondence between a force point and an image (beginning, middle or end of a jump) has to be taken into account if one wants to look at short time effects (i.e. on the order of the minimal pulse duration possible). Here, we chose to align the beginning of the pulse for simplicity.

#### 4.4.2. Other sources of excitation

Such a coupling signal can be also observed with lasers, and even in TIRF mode of illumination (C.M. Franz, personal communication). Tests have shown that the use of an HBO source using the Colibri as a shutter created a mechanical noise of rather large intensity as compared to the coupling signal, preventing its use (not shown).

#### 4.4.3. Cantilevers without coating

When modifying the coating of the levers, precautions have to be taken to verify that (i) such levers have a sufficient reflectivity

for the AFM to perform reliable measurements and (ii) since they are more "transparent", that the levels of infra-red or red light that pass through and hit the cell is not perturbing it. On the set-up used here, with commercial gold less levers or made using chemical attack, reflectivity was good enough to achieve a good signal to noise ratio and the IR laser did not seem to have strong effects onto the tested cells, loaded or not with fluorescent reporters, as inferred from their shape and behaviour.

#### 4.4.4. Ratiometric or FRET imaging

We tested the superimposition of 470 nm/555 nm lights, simultaneously or one after the other, and observed that the resulting signals are additive and stay of low magnitude for uncoated levers (Supplementary Fig. 5). This opens, for example, the use of Fluo4/FuraRed mixture as a way to perform, easily, with a single detection channel, ratiometric calcium measurements. For more complex signal reporters, such as Fura2 or even FRET dyes such as ROZA, a reporter of Zap70 activation [29], the combination with a DualView detection system (DV2, Photometrics, http://www.photometrics.com), allowing the simultaneous detection of two wavelengths without any mobile part, on the same camera, could prove a rather easy implementation, using the coupling signal as an reliable timer.

### 4.5. Perspectives: stimulations using specific molecules

The present experiments open the way to mechanical (with bare beads) or specific (with beads grafted with specific, density controlled and oriented molecules) stimulation experiments. Controlling the bead size, specific molecule grafting density, indentation force, contact time, and recording the indentation depth may allow to gain a fine control on the number of molecules that are presented to the tested cell. If the recognition/adhesion events are long-lived enough and create solid bonds, the pulling part of the force curves may be compared to this number thanks to a detailed analysis of the rupture events along the separation, opening exciting new perspectives in the field of Single Cell Force Spectroscopy-based techniques [2,6,52–55].

## 5. Conclusion

A coupling signal existing between AFM and fluorescence microscopy, manifesting as a bending of the AFM cantilever upon shinning excitation light, has been described. It has been characterized in terms of duration, periodicity and intensity, as a function of excitation wavelength and power, for four different types of soft cantilevers that are commonly used in biological applications of AFM force mode. Three different geometries and rigidities ($<100$ pN/nm) were examined. For commercial uncoated levers, this signal is of moderate intensity ($\sim$50–100 pN), reproducible, and can hence be used as an intrinsic timer for real-time use of AFM and epifluorescence.

This approach presents the advantage of avoiding the needs of a physical connection between the AFM computer and the fluorescence detection system to synchronize the observed signals (force on one side and fluorescence images on the other side).

Two applications were presented, namely (i) single immune cell mechanical stimulation while following the consequences of the contact via fluorescent calcium reporters and (ii) single T cell stimulation by light, using a photoactivable Rac protein, while recording the mechanical consequences of this activation.

The present study highlights the precautions of use and limitations, in particular discussing the time resolution (number of frames per second, duration of the excitation). Modifications of the set-up have been proposed to enlarge this approach to more complex, dual wavelengths dyes (such as ratiometric calcium dyes or FRET reporters), together with optimizing the geometry of the mechanical contact by modifying the levers.

The mechanical stimulation experiments are paving the way to specific stimulations where a given molecule will be oriented, at a known density, grafted on the bead modified lever, to represent a model APC. Physical/mechanical parameters of the contact (duration, frequency, force, rigidity of the lever i.e. apparent APC rigidity [51]) could then be varied in order to decipher the transfer function of given pathways encoding the information received at the membrane and transmitted to the cytosol, exploiting the fluorescence recording in real-time or relevant markers. Such a simple technique may open the use of AFM to dissect mechanochemistry at single cell level, by allowing forces and their consequences to be easily correlated.

Two exquisite systems of uttermost importance in immunology would be by targeting the TCR and/or other activating/adhesive molecules on T cells, and following the consequences of the interaction between the antibody Fc fragment and its receptor (FcR) using suitably opsonized beads of various sizes in the macrophage context.

## Contributions

PHP designed, performed experiments, processed the data and wrote the article. MBP performed the plasmid transfection and stimulation experiments. SC, AS, MM, SO performed experiments and processed the data. LL performed experiments and participated in writing the article. PB participated to the design of the study and in writing the article.

## Acknowledgements

*Fundings*: Prise de Risques CNRS, ANR JCJC "DissecTion" (ANR-09-JCJC-0091), PhysCancer "H+-cancer" (to PHP). Labex INFORM (ANR-11-LABX-0054) and A*MIDEX project (ANR-11-IDEX-0001-02), funded by the "Investissements d'Avenir" French Government program managed by the French National Research Agency (ANR) (to Inserm U1067 Lab and as PhD grant to AS). GDR MIV (as a master grant to SO).

*Providing material or technical help*: P. Robert (U1067, Marseille), Y. Hamon and H.-T. He (CIML, Marseille, France). A. Dumêtre (UMD3, Marseille, France) [J774 cells], K. Hahn [Rac–PA plasmid], F. Bedu and H. Dallaporta (CINAM, Marseille) [ion beam cutting]. F. Eghiaian, A. Rigato and F. Rico (U1006, Marseille) [chemical gold removal recipes and discussions]. P. Dumas (CINAM, Marseille) [discussions]. R. Fabre (CIML, Marseille) [preliminary experiments].

*Companies*: JPK Instruments (Berlin, Germany) for continuous support and generous help. Zeiss France for support.

## Appendix A. Supplementary material

Supplementary data associated with this article can be found in the online version at http://dx.doi.org/10.1016/j.ultramic.2015.10.014.

## References

[1] C.M. Franz, P.-H. Puech, et al., Atomic force microscopy: a versatile tool for studying cell morphology, adhesion and mechanics, Cell. Mol. Bioeng. 1 (4) (2008) 289–300.

[2] Y.F. Dufrêne, E. Evans, A. Engel, J. Helenius, H.E. Gaub, D.J. Müller, et al., Five challenges to bringing single-molecule force spectroscopy into living cells, Nat. Methods 8 (2) (2011) 123–127.

[3] P. Hinterdorfer, W. Baumgartner, H.J. Gruber, K. Schilcher, H. Schindler, et al., Detection and localization of individual antibody–antigen recognition events by atomic force microscopy, Proc. Natl. Acad. Sci. U.S.A. 93 (8) (1996) 3477–3481.

[4] V.T. Moy, E.L. Florin, H.E. Gaub, et al., Intermolecular forces and energies between ligands and receptors, Science 266 (5183) (1994) 257–259.

[5] C.M. Franz, A. Taubenberger, P.-H. Puech, D.J. Muller, et al., Studying integrin-mediated cell adhesion at the single-molecule level using AFM force spectroscopy, Sci. STKE Signal Transduct. Knowl. Environ. 2007 (406) (2007) l5.

[6] J. Helenius, C.-P. Heisenberg, H.E. Gaub, D.J. Muller, et al., Single-cell force spectroscopy, J. Cell. Sci. 121 (Pt 11) (2008) 1785–1791.

[7] P.-H. Puech, K. Poole, D. Knebel, D.J. Muller, et al., A new technical approach to quantify cell–cell adhesion forces by AFM, Ultramicroscopy 106 (8–9) (2006) 637–644.

[8] J.B. Huppa, M.M. Davis, et al., Chapter One – the interdisciplinary science of T-cell recognition, in: F.W. Alt (Ed.), Advances in Immunology, vol. 119, Academic Press, 2013, pp. 1–50.

[9] P.-H. Puech, D. Nevoltris, P. Robert, L. Limozin, C. Boyer, P. Bongrand, et al., Force measurements of TCR/pMHC recognition at T cell surface, PLoS One 6 (7) (2011) e22344.

[10] E. Natkanski, W.-Y. Lee, B. Mistry, A. Casal, J.E. Molloy, P. Tolar, et al., B cells use mechanical energy to discriminate antigen affinities, Science 340 (6140) (2013) 1587–1590.

[11] H.-T. He, P. Bongrand, et al., Membrane dynamics shape TCR-generated signaling, Front. Immunol. 3 (2012) 90.

[12] S.T. Kim, K. Takeuchi, Z.-Y.J. Sun, M. Touma, C.E. Castro, A. Fahmy, M.J. Lang, G. Wagner, E.L. Reinherz, et al., The alphabeta T cell receptor is an anisotropic mechanosensor, J. Biol. Chem. 284 (45) (2009) 31028–31037.

[13] S.T. Kim, Y. Shin, K. Brazin, R.J. Mallis, Z.-Y.J. Sun, G. Wagner, M.J. Lang, E. L. Reinherz, et al., TCR mechanobiology: torques and tunable structures linked to early T cell signaling, Front. Immunol. 3 (2012) 76.

[14] Y.-C. Li, B.-M. Chen, P.-C. Wu, T.-L. Cheng, L.-S. Kao, M.-H. Tao, A. Lieber, S. R. Roffler, et al., Cutting edge: mechanical forces acting on T cells immobilized via the TCR complex can trigger TCR signaling, J. Immunol. (Balt. MD. 1950) 184 (11) (2010) 5959–5963.

[15] Z. Ma, T.H. Finkel, et al., T cell receptor triggering by force, Trends Immunol. 31 (1) (2010) 1–6.

[16] Z. Ma, D.E. Discher, T.H. Finkel, et al., Mechanical force in T cell receptor signal initiation, Front. Immunol. 3 (2012) 217.

[17] R. Merkel, P. Nassoy, A. Leung, K. Ritchie, E. Evans, et al., Energy landscapes of receptor–ligand bonds explored with dynamic force spectroscopy, Nature, 397, (1999) 50–53.

[18] A. Pierres, A.-M. Benoliel, P. Bongrand, et al., Studying molecular interactions at the single bond level with a laminar flow chamber, Cell. Mol. Bioeng. 1 (4) (2008) 247–262.

[19] B. Liu, W. Chen, B.D. Evavold, C. Zhu, et al., Accumulation of dynamic catch bonds between TCR and agonist peptide-MHC triggers T cell signaling, Cell 157 (2) (2014) 357–368.

[20] P. Robert, M. Aleksic, O. Dushek, V. Cerundolo, P. Bongrand, P.A. van der Merwe, et al., Kinetics and mechanics of two-dimensional interactions between T cell receptors and different activating ligands, Biophys. J. 102 (2) (2012) 248–257.

[21] S. Hoffmann, B.H. Hosseini, M. Hecker, I. Louban, N. Bulbuc, N. Garbi, G. H. Wabnitz, Y. Samstag, J.P. Spatz, G.J. Hämmerling, et al., Single cell force spectroscopy of T cells recognizing a myelin-derived peptide on antigen presenting cells, Immunol. Lett. 136 (1) (2011) 13–20.

[22] B.H. Hosseini, I. Louban, D. Djandji, G.H. Wabnitz, J. Deeg, N. Bulbuc, Y. Samstag, M. Gunzer, J.P. Spatz, G.J. Hämmerling, et al., Immune synapse formation determines interaction forces between T cells and antigen-presenting cells measured by atomic force microscopy, Proc. Natl. Acad. Sci. U.S.A. 106 (42) (2009) 17852–17857.

[23] W. Chen, C. Zhu, et al., Mechanical regulation of T-cell functions, Immunol. Rev. 256 (1) (2013) 160–176.

[24] M.L. Previtera, Mechanotransduction in the immune system, Cell. Mol. Bioeng. 7 (3) (2014) 473–481.

[25] A. Brodovitch, P. Bongrand, A. Pierres, et al., T lymphocytes sense antigens within seconds and make a decision within one minute, J. Immunol. 191 (5) (2013) 2064–2071.

[26] E. Judokusumo, E. Tabdanov, S. Kumari, M.L. Dustin, L.C. Kam, et al., Mechanosensing in T lymphocyte activation, Biophys. J. 102 (2) (2012) L5–L7.

[27] A. Salles, C. Billaudeau, A. Sergé, A.-M. Bernard, M.-C. Phélipot, N. Bertaux, M. Fallet, P. Grenot, D. Marguet, H.-T. He, Y. Hamon, et al., Barcoding T cell calcium response diversity with methods for automated and accurate analysis of cell signals (MAAACS), PLoS Comput. Biol. 9 (9) (2013) e1003245.

[28] C. Torigoe, T. Tadakuma, M. Nakanishi, et al., Single-cell observation of calcium signals in T cells and antigen-presenting cells during antigen presentation, Immunol. Lett. 46 (1–2) (1995) 75–79.

[29] C. Randriamampita, P. Mouchacca, B. Malissen, D. Marguet, A. Trautmann, A. C. Lellouch, et al., A novel ZAP-70 dependent FRET based biosensor reveals kinase activity at both the immunological synapse and the antisynapse, PLoS One 3 (1) (2008) e1521.

[30] G.T. Charras, M.A. Horton, et al., Single cell mechanotransduction and its modulation analyzed by atomic force microscope indentation, Biophys. J. 82 (6) (2002) 2970–2981.

[31] J. Husson, K. Chemin, A. Bohineust, C. Hivroz, N. Henry, et al., Force generation upon T cell receptor engagement, PLoS One 6 (5) (2011) e19680.

[32] G.T. Charras, P.P. Lehenkari, M.A. Horton, et al., Atomic force microscopy can be used to mechanically stimulate osteoblasts and evaluate cellular strain distributions, Ultramicroscopy 86(1–2) (2001) 85–95.

[33] G.M. Lopez-Ayon, D.J. Oliver, P.H. Grutter, S.V. Komarova, et al., Deconvolution of calcium fluorescent indicator signal from AFM cantilever reflection, Microsc. Microanal. J. Microsc. Soc. Am. Microbeam Anal. Soc. Microsc. Soc. Can. 18 (4) (2012) 808–815.

[34] Y.-S. Chu, W.A. Thomas, O. Eder, F. Pincet, E. Perez, J.P. Thiery, S. Dufour, et al., Force measurements in E-cadherin-mediated cell doublets reveal rapid adhesion strengthened by actin cytoskeleton remodeling through Rac and Cdc42, J. Cell. Biol. 167 (6) (2004) 1183–1194.

[35] P. Robert, K. Sengupta, P.-H. Puech, P. Bongrand, L. Limozin, et al., Tuning the formation and rupture of single ligand–receptor bonds by hyaluronan-induced repulsion, Biophys. J. 95 (8) (2008) 3999–4012.

[36] J. Te Riet, J. Helenius, N. Strohmeyer, A. Cambi, C.G. Figdor, D.J. Müller, et al., Dynamic coupling of ALCAM to the actin cortex strengthens cell adhesion to CD6, J. Cell. Sci. 127 (Pt 7) (2014) 1595–1606.

[37] A.R. Harris, G.T. Charras, et al., Experimental validation of atomic force microscopy-based cell elasticity measurements, Nanotechnology 22 (34) (2011) 345102.

[38] Y.I. Wu, D. Frey, O.I. Lungu, A. Jaehrig, I. Schlichting, B. Kuhlman, K.M. Hahn, et al., A genetically encoded photoactivatable Rac controls the motility of living cells, Nature 461 (7260) (2009) 104–108.

[39] H.-J. Butt, M. Jaschke, et al., Calculation of thermal noise in atomic force microscopy, Nanotechnology 6 (1) (1995) 1.

[40] B. Olher, Practical advice on the determination of cantilever spring constants (Application note AN94), Bruker (ex. VeecoInstruments), 2007.

[41] A. Edelstein, N. Amodaj, K. Hoover, R. Vale, N. Stuurman, et al., Computer control of microscopes using μManager, in: M. Frederick, Al Ausubel (Eds.), Curr. Protoc. Mol. Biol. Ed., Chapter 14, Unit 14.20, 2010.

[42] J. Schindelin, I. Arganda-Carreras, E. Frise, V. Kaynig, M. Longair, T. Pietzsch, S. Preibisch, C. Rueden, S. Saalfeld, B. Schmid, J.-Y. Tinevez, D.J. White, V. Hartenstein, K. Eliceiri, P. Tomancak, A. Cardona, et al., Fiji: an open-source platform for biological-image analysis, Nat. Methods 9 (7) (2012) 676–682.

[43] F. Rico, C. Chu, M.H. Abdulreda, Y. Qin, V.T. Moy, et al., Temperature modulation of integrin-mediated cell adhesion, Biophys. J. 99 (5) (2010) 1387–1396.

[44] E.P. Wojcikiewicz, X. Zhang, A. Chen, V.T. Moy, et al., Contributions of molecular binding events and cellular compliance to the modulation of leukocyte adhesion, J. Cell. Sci. 116 (Pt 12) (2003) 2531–2539.

[45] N. Bufi, M. Saitakis, S. Dogniaux, O. Buschinger, A. Bohineust, A. Richert, M. Maurin, C. Hivroz, A. Asnacios, et al., Human primary immune cells exhibit distinct mechanical properties that are modified by inflammation, Biophys. J. 108 (9) (2015) 2181–2190.

[46] H.W. Wu, T. Kuhn, V.T. Moy, et al., Mechanical properties of L929 cells measured by atomic force microscopy: effects of anticytoskeletal drugs and membrane crosslinking, Scanning 20 (5) (1998) 389–397.

[47] M. Herant, V. Heinrich, M. Dembo, et al., Mechanics of neutrophil phagocytosis: experiments and quantitative models, J. Cell. Sci. 119 (9) (2006) 1903–1913.

[48] A.B. Churnside, R.M.A. Sullan, D.M. Nguyen, S.O. Case, M.S. Bull, G.M. King, T. T. Perkins, et al., Routine and timely sub-piconewton force stability and precision for biological applications of atomic force microscopy, Nano Lett. 12 (7) (2012) 3557–3561.

[49] M. Radmacher, J.P. Cleveland, P.K. Hansma, et al., Improvement of thermally induced bending of cantilevers used for atomic force microscopy, Scanning 17 (2) (1995) 117–121.

[50] M.S. Bull, R.M.A. Sullan, H. Li, T.T. Perkins, et al., Improved single molecule force spectroscopy using micromachined cantilevers, ACS Nano 8 (5) (2014) 4984–4995.

[51] D. Mitrossilis, J. Fouchard, D. Pereira, F. Postic, A. Richert, M. Saint-Jean, A. Asnacios, et al., Real-time single-cell response to stiffness, Proc. Natl. Acad. Sci. U.S.A. 107 (38) (2010) 16518–16523.

[52] J. Kashef, C.M. Franz, Quantitative methods for analyzing cell–cell adhesion in development, Dev. Biol. 401 (1) (2015) 165–174.

[53] A.V. Taubenberger, D.W. Hutmacher, D.J. Muller, Single-cell force spectroscopy, an emerging tool to quantify cell adhesion to biomaterials, Tissue Eng. Part B Rev. 20 (1) (2014) 40–55.

[54] J. Friedrichs, K.R. Legate, R. Schubert, M. Bharadwaj, C. Werner, D.J. Müller, M. Benoit, A practical guide to quantify cell adhesion using single-cell force spectroscopy, Methods 60 (2) (2013) 169–178.

[55] D.J. Müller, J. Helenius, D. Alsteens, Y.F. Dufrêne, Force probing surfaces of living cells to molecular resolution, Nat. Chem. Biol. 5 (6) (2009) 383–390.